Journal of Solid Mechanics Vol. 8, No. 2 (2016) pp. 280-299

Bending Analysis of Composite Sandwich Plates with Laminated Face Sheets: New Finite Element Formulation

M. O. Belarbi *, A. Tati

Laboratoire de Génie Energétique et Matériaux, LGEM. Université de Biskra, B.P. 145, R.P. 07000, Biskra, Algeria

Received 12 February 2016; accepted 27 March 2016

ABSTRACT

The bending behavior of composites sandwich plates with multi-layered laminated face sheets has been investigated, using a new four-nodded rectangular finite element formulation based on a layer-wise theory. Both, first order and higher-order shear deformation; theories are used in order to model the face sheets and the core, respectively. Unlike any other layer-wise theory, the number of degrees of freedom in this present model is independent of the number of layers. The compatibility conditions as well as the displacement continuity at the interface 'face sheets–core' are satisfied. In the proposed model, the three translation components are common for the all sandwich layers, and are located at the mid-plane of the sandwich plate. The obtained results show that the developed model is able to give accurate transverse shear stresses directly from the constitutive equations. Moreover, a parametric study was also conducted to investigate the effect of certain characteristic parameters (core thickness to total thickness ratio, side-to-thickness ratio, boundary conditions, plate aspect ratio, core-to-face sheet anisotropy ratio, core shear modulus to the flexural modulus ratio and degree of orthotropy of the face sheet) on the transverse displacement variation. The numerical results obtained by our model are compared favorably with those obtained via analytical solution and numerical/experimental, results obtained by other models. The results obtained from this investigation will be useful for a more comprehensive understanding of the behavior of sandwich laminates.

Keywords : Layer-wise; Finite element; Sandwich plates; Bending.

1 INTRODUCTION

CURRENTLY, composite sandwich structures gained considerable attention and became increasingly important in different engineering fields (e.g. civil, aerospace, marine), due to their rigidity-and-resistance to weight ratios. However, there are still questions on the complexity of the behavior of these structures. The effect of shear deformation is quite significant which may lead to failure and becomes more complex in case of sandwich construction, as the material property variation is very large between the core and face layers [1]. Moreover, an accurate estimation of stress components, specifically the transverse shear stresses, plays an important role in reducing these failures [2].

In the literature, several two-dimensional theories have been proposed to study the behavior of composite sandwich structures. Starting by the simple classical laminated plate theory (CLPT), based on the Kirchhoff's assumptions [3], which does not includes the effect of the transverse shear deformation [4-6], the first order shear

*Corresponding author. Tel.: +213 772 55 65 61.
E-mail address: mo.belarbi@univ-biskra.dz (M.O.Belarbi).

deformation theory (FSDT), where the effect of the transverse shear deformation is considered [7-10], but taken constant through the thickness, and the higher order shear deformation theories (HSDT) where a better representation of transverse shear effect can be obtained [11-16]. All these theories falls within the equivalent single layers (ESL) theories.

However, the ESL approach is unable to predict accurately the local behavior (e.g. interlaminar stresses) of sandwich structures. For that reason, many researchers developed more accurate theories such as the zig–zag theories (ZZT) [1, 17-22] and the global-local higher order shear deformation theories (GLHSDT) [23-27]. Recently, various works have adopted the layer-wise theories (LW) [28-37] to assume separate displacement field expansions within each material layer, thus providing a kinematically correct representation of the strain field in discrete laminated layer, and allowing accurate determination of ply level stresses [38]. For more details the reader may refer to [38-43].

In the finite elements development, many researchers have adopted the layer-wise theory for the sake of a good description of sandwich structures. On this topic, we can distinguish the work of Wu and Lin [35] where a two-dimensional mixed finite element based on higher order layer-wise model is presented for the analysis of thick sandwich plates. The displacement continuity at the interface is satisfied as well as the interlaminar stresses. These authors proposed for each layer, a cubic and quadratic polynomial functions for in-plane and transverse displacements, respectively. Afterwards, Lee and Fan [28] describe a new model using the first order shear deformation theory for the face sheets, whereas the displacement field at the core is expressed in terms of the two face sheets displacements. In this model, the transverse shear strain varies linearly while the transverse normal strain is constant through the thickness of the core. They used a nine-nodded isoparametric finite element to study the bending and vibration of sandwich plates. On the other hand, a three-dimensional (3D), layer-wise finite element model was developed by Oskooei and Hansen [31] to analyze the sandwich plates with laminated face sheets. They used the first order shear deformation theory for the face sheets, whereas for the core a cubic and quadratic, functions for the in-plane and transverse, displacements, was adopted. In addition, an eighteen-node three-dimensional brick mixed finite element with six degrees of freedom (6 DOF) per node based on layer-wise theory has been developed by Ramtekkar et al. [44, 45] for an accurate evaluation of transverse stresses in laminated sandwich. In this model, the continuity of displacements as well as the transverse stresses is satisfied. In the same context, Linke et al. [29] developed a three-dimensional displacement finite element containing eleven DOF at each node (each face-sheet contains five DOF per node and only one DOF in the core) for static and stability analysis of sandwich plates. The formulation of this element is based on the layer-wise approach, where the face sheets are represented as an elements of classical plate theory and the core is represented by the third order shear deformation theory (TSDT). The in and out-of, plane displacements of the core assume a cubic and quadratic variation, respectively. Later, a forty-five nodes triangular element having seven DOF per node was developed by Ramesh et al. [33] for accurate prediction of interlaminar stresses in laminated composite plates. The construction of this element is based on two theories; the third order shear deformation theory and the layer-wise plate theory of Reddy [34]. Recently, Mantari et al. [30] presented a new layer-wise model using a trigonometric displacement field for in-plane displacements and constant out-of plane displacements through the thickness. The authors used a C^0 four-node isoparametric quadrilateral element to study the bending of thick sandwich panels.

In the present paper, the bending behavior of sandwich plates with laminated composites face sheets has been investigated by using a new four-nodded rectangular finite element formulation based on a layer-wise theory. The face sheets are modeled based on the first order shear deformation theory, whereas the core is modeled using the third-order shear deformation plate theory. Unlike any other layer-wise theory, the number of degrees of freedom is independent of the number of layers. The performance of the proposed formulation is assessed by several study cases, considering different aspect ratios, loadings and boundary conditions. The obtained numerical results can be compared with the analytical solutions given by Pagano [46], the experimental results obtained by Kanematsu et al. [47] and the numerical results found by finite elements models [1, 17, 18, 22]. The second objective of this paper is to investigate the influence of material property parameters and plate geometry variables on the transverse displacement.

2 MATHEMATICAL MODEL

Sandwich plate is a structure composed of three principal layers, as shown in Fig.1, two face sheets (top-bottom) of thicknesses $(h_t),(h_b)$ respectively, and a central layer named core of thickness (h_c) which is thicker than the

previous ones. Total thickness (h) of the plate is the sum of these thicknesses. The plane (x, y) coordinate system coincides with mi-plane plate.

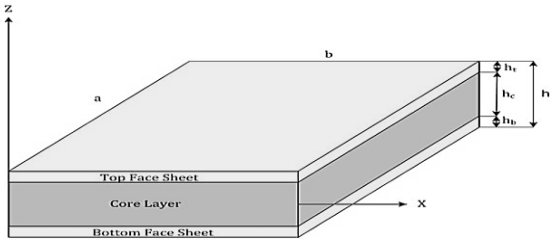

Fig.1
Geometry and notations of a sandwich plate.

2.1 Kinematic assumptions for the core

In the proposed model, the core is modeled using the third-order shear deformation theory (TSDT). The through-thickness variation of in-plane displacements (*u* and *v*) and transverse displacement (*w*) may be expressed, respectively as follows:

$$u_c = u_0 + z\psi_x^c + z^2\eta_x^c + z^3\zeta_x^c \qquad ,v_c = v_0 + z\psi_y^c + z^2\eta_y^c + z^3\zeta_y^c \qquad ,w_c = w_0 \tag{1}$$

where u_0, v_0 and w_0 are respectively, in-plane and transverse displacement components at the mid-plane of the sandwich plate. ψ_x^c, ψ_y^c represent normal rotations about the *x* and *y* axis respectively. The parameters $\eta_x^c, \eta_y^c, \zeta_x^c$ and ζ_y^c are higher order terms.

The strain-displacement relationships can be written in the following form

$$\begin{aligned} &\varepsilon_{xx} = \varepsilon_x^{(0)} + z\,\chi_x^{(1)} + z^2\chi_x^{(2)} + z^3\chi_x^{(3)} \qquad ,\varepsilon_{yy} = \varepsilon_y^{(0)} + z\,\chi_y^{(1)} + z^2\chi_y^{(2)} + z^3\chi_y^{(3)} \\ &\gamma_{xy} = \gamma_{xy}^{(0)} + z\,\chi_{xy}^{(1)} + z^2\chi_{xy}^{(2)} + z^3\chi_{xy}^{(3)} \qquad ,\gamma_{yz} = \gamma_{yz}^{(0)} + z\,\chi_{yz}^{(1)} + z^2\chi_{yz}^{(2)} \qquad ,\gamma_{xz} = \gamma_{xz}^{(0)} + z\,\chi_{xz}^{(1)} + z^2\chi_{xz}^{(2)} \end{aligned} \tag{2}$$

where,

$$\begin{aligned} &\varepsilon^{(0)} = \left(\varepsilon_x^{(0)}, \varepsilon_y^{(0)}, \gamma_{xy}^{(0)}\right) = \left(\frac{\partial u_0}{\partial x}, \frac{\partial v_0}{\partial y}, \frac{\partial u_0}{\partial y} + \frac{\partial v_0}{\partial x}\right) \\ &\chi^{(1)} = \left(\chi_x^{(1)}, \chi_y^{(1)}, \chi_{xy}^{(1)}\right) = \left(\frac{\partial \psi_x^c}{\partial x}, \frac{\partial \psi_y^c}{\partial y}, \frac{\partial \psi_x^c}{\partial y} + \frac{\partial \psi_y^c}{\partial x}\right) \\ &\chi^{(2)} = \left(\chi_x^{(2)}, \chi_y^{(2)}, \chi_{xy}^{(2)}\right) = \left(\frac{\partial \eta_x^c}{\partial x}, \frac{\partial \eta_y^c}{\partial y}, \frac{\partial \eta_x^c}{\partial y} + \frac{\partial \eta_y^c}{\partial x}\right) \\ &\chi^{(3)} = \left(\chi_x^{(3)}, \chi_y^{(3)}, \chi_{xy}^{(3)}\right) = \left(\frac{\partial \zeta_x^c}{\partial x}, \frac{\partial \zeta_y^c}{\partial y}, \frac{\partial \zeta_x^c}{\partial y} + \frac{\partial \zeta_y^c}{\partial x}\right) \\ &\gamma_s^{(0)} = \left(\gamma_{yz}^{(0)}, \gamma_{xz}^{(0)}\right) = \left(\psi_y^c + \frac{\partial w_0}{\partial y}, \psi_x^c + \frac{\partial w_0}{\partial x}\right) \\ &\chi_s^{(1)} = \left(\chi_{yz}^{(1)}, \chi_{xz}^{(1)}\right) = \left(2\eta_y^c, 2\eta_x^c\right) \qquad \chi_s^{(2)} = \left(\chi_{yz}^{(2)}, \chi_{xz}^{(2)}\right) = \left(3\zeta_y^c, 3\zeta_x^c\right) \end{aligned} \tag{3}$$

2.2 Kinematic assumptions for the face sheets

The face sheets are modeled using the first-order shear deformation theory (FSDT). The compatibility conditions as well as the displacement continuity at the interface (top face-sheet, core, bottom face-sheet), leads to the following improved displacement fields (Fig. 2)

a. Top face-sheet

$$u_t = u_c\left(\frac{h_c}{2}\right)+\left(z-\frac{h_c}{2}\right)\psi_x^t \qquad ,v_t = v_c\left(\frac{h_c}{2}\right)+\left(z-\frac{h_c}{2}\right)\psi_y^t \qquad ,w_t = w_0 \tag{4}$$

where ψ_x^t and ψ_y^t are the rotations of the top face-sheet cross section about the *x* and *y* axis, respectively. with,

$$u_c\left(\frac{h_c}{2}\right) = u_0 + \left(\frac{h_c}{2}\right)\psi_x^c + \left(\frac{h_c^2}{4}\right)\eta_x^c + \left(\frac{h_c^3}{8}\right)\zeta_x^c \qquad ,v_c = v_0 + \left(\frac{h_c}{2}\right)\psi_y^c + \left(\frac{h_c^2}{4}\right)\eta_y^c + \left(\frac{h_c^3}{8}\right)\zeta_y^c \tag{5}$$

Substitution of Eq. (5) into Eq. (4) leads to the following expression

$$\begin{aligned} u_t &= u_0 + \left(\frac{h_c}{2}\right)\psi_x^c + \left(\frac{h_c^2}{4}\right)\eta_x^c + \left(\frac{h_c^3}{8}\right)\zeta_x^c + \left(z-\frac{h_c}{2}\right)\psi_x^t \\ v_t &= v_0 + \left(\frac{h_c}{2}\right)\psi_y^c + \left(\frac{h_c^2}{4}\right)\eta_y^c + \left(\frac{h_c^3}{8}\right)\zeta_y^c + \left(z-\frac{h_c}{2}\right)\psi_y^t \qquad w_t = w_0 \end{aligned} \tag{6}$$

b. Bottom face-sheet

According to Fig. 2, the displacement field of the bottom face sheet can be written as:

$$u_b = u_c\left(-\frac{h_c}{2}\right)+\left(z+\frac{h_c}{2}\right)\psi_x^b \qquad ,v_b = v_c\left(-\frac{h_c}{2}\right)+\left(z+\frac{h_c}{2}\right)\psi_y^b \qquad ,w_b = w_0 \tag{7}$$

where ψ_x^b and ψ_y^b are the rotations of the bottom face-sheet cross section about the *y* and *x* axis respectively where,

$$u_c\left(-\frac{h_c}{2}\right) = u_0 - \left(\frac{h_c}{2}\right)\psi_x^c + \left(\frac{h_c^2}{4}\right)\eta_x^c - \left(\frac{h_c^3}{8}\right)\zeta_x^c \qquad v_c\left(-\frac{h_c}{2}\right) = v_0 - \left(\frac{h_c}{2}\right)\psi_y^c + \left(\frac{h_c^2}{4}\right)\eta_y^c - \left(\frac{h_c^3}{8}\right)\zeta_y^c \tag{8}$$

Substituting Eq. (8) into Eq. (7), leads to the following expression

$$\begin{aligned} u_b &= u_0 - \left(\frac{h_c}{2}\right)\psi_x^c + \left(\frac{h_c^2}{4}\right)\eta_x^c - \left(\frac{h_c^3}{8}\right)\zeta_x^c + \left(z+\frac{h_c}{2}\right)\psi_x^b \\ v_b &= v_0 - \left(\frac{h_c}{2}\right)\psi_y^c + \left(\frac{h_c^2}{4}\right)\eta_y^c - \left(\frac{h_c^3}{8}\right)\zeta_y^c + \left(z+\frac{h_c}{2}\right)\psi_y^b \qquad w_b = w_0 \end{aligned} \tag{9}$$

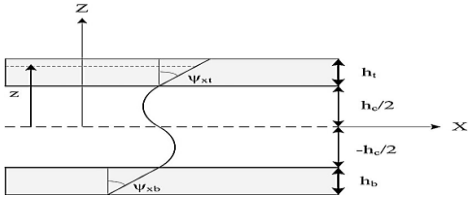

Fig.2
Kinematics.

2.2.1 Strains

The strain-displacement relationships of the top face-sheet are given by

$$\begin{aligned}
\varepsilon_{xx}^{t} &= \frac{\partial u_t}{\partial x} = \frac{\partial u_0}{\partial x} + \left(\frac{h_c}{2}\right)\frac{\partial \psi_x^c}{\partial x} + \left(\frac{h_c^2}{4}\right)\frac{\partial \eta_x^c}{\partial x} + \left(\frac{h_c^3}{8}\right)\frac{\partial \zeta_x^c}{\partial x} + (z-\frac{h_c}{2})\frac{\partial \psi_x^t}{\partial x} \\
\varepsilon_{yy}^{t} &= \frac{\partial v_t}{\partial y} = \frac{\partial v_0}{\partial y} + \left(\frac{h_c}{2}\right)\frac{\partial \psi_y^c}{\partial y} + \left(\frac{h_c^2}{4}\right)\frac{\partial \eta_y^c}{\partial y} + \left(\frac{h_c^3}{8}\right)\frac{\partial \zeta_y^c}{\partial y} + (z-\frac{h_c}{2})\frac{\partial \psi_y^t}{\partial y} \\
\gamma_{xy}^{t} &= \frac{\partial u_t}{\partial y} + \frac{\partial v_t}{\partial x} = \left(\frac{\partial u_0}{\partial y} + \frac{\partial v_0}{\partial x}\right) + \frac{h_c}{2}\left(\frac{\partial \psi_x^c}{\partial y} + \frac{\partial \psi_y^c}{\partial x}\right) + \frac{h_c^2}{4}\left(\frac{\partial \eta_x^c}{\partial y} + \frac{\partial \eta_y^c}{\partial x}\right) + \frac{h_c^3}{8}\left(\frac{\partial \zeta_x^c}{\partial y} + \frac{\partial \zeta_y^c}{\partial x}\right) + (z-\frac{h_c}{2})\left(\frac{\partial \psi_x^t}{\partial y} + \frac{\partial \psi_y^t}{\partial x}\right) \\
\gamma_{yz}^{t} &= \frac{\partial w_0}{\partial y} + \psi_y^t \qquad \gamma_{xz}^{t} = \frac{\partial w_0}{\partial x} + \psi_x^t
\end{aligned} \tag{10}$$

The strain-displacement relationships of the bottom face-sheet can be written in the following form

$$\begin{aligned}
\varepsilon_{xx}^{b} &= \frac{\partial u_b}{\partial x} = \frac{\partial u_0}{\partial x} - \left(\frac{h_c}{2}\right)\frac{\partial \psi_x^c}{\partial x} + \left(\frac{h_c^2}{4}\right) - \frac{\partial \eta_x^c}{\partial x}\left(\frac{h_c^3}{8}\right)\frac{\partial \zeta_x^c}{\partial x} + (z+\frac{h_c}{2})\frac{\partial \psi_x^b}{\partial x} \\
\varepsilon_{yy}^{b} &= \frac{\partial v_b}{\partial y} = \frac{\partial v_0}{\partial y} - \left(\frac{h_c}{2}\right)\frac{\partial \psi_y^c}{\partial y} + \left(\frac{h_c^2}{4}\right) - \frac{\partial \eta_y^c}{\partial y}\left(\frac{h_c^3}{8}\right)\frac{\partial \zeta_y^c}{\partial y} + (z+\frac{h_c}{2})\frac{\partial \psi_y^b}{\partial y} \\
\gamma_{xy}^{b} &= \frac{\partial u_b}{\partial y} + \frac{\partial v_b}{\partial x} = \left(\frac{\partial u_0}{\partial y} + \frac{\partial v_0}{\partial x}\right) - \frac{h_c}{2}\left(\frac{\partial \psi_x^c}{\partial y} + \frac{\partial \psi_y^c}{\partial x}\right) + \frac{h_c^2}{4}\left(\frac{\partial \eta_x^c}{\partial y} + \frac{\partial \eta_y^c}{\partial x}\right) - \frac{h_c^3}{8}\left(\frac{\partial \zeta_x^c}{\partial y} + \frac{\partial \zeta_y^c}{\partial x}\right) + (z+\frac{h_c}{2})\left(\frac{\partial \psi_x^b}{\partial y} + \frac{\partial \psi_y^b}{\partial x}\right) \\
\gamma_{yz}^{b} &= \frac{\partial w_0}{\partial y} + \psi_y^b \qquad \gamma_{xz}^{b} = \frac{\partial w_0}{\partial x} + \psi_x^b
\end{aligned} \tag{11}$$

2.3 Constitutive relationships

In this paper, the two face sheets (top and bottom) are considered as laminated composite, as shown in Fig. 3. So, the stress-strain relationship of the k^{th} layer in the global coordinate system is given by

$$\begin{Bmatrix} \sigma_x^f \\ \sigma_y^f \\ \tau_{yz}^f \\ \tau_{xz}^f \\ \tau_{xy}^f \end{Bmatrix}_k = \begin{bmatrix} \overline{Q_{11}} & \overline{Q_{12}} & 0 & 0 & \overline{Q_{16}} \\ \overline{Q_{21}} & \overline{Q_{22}} & 0 & 0 & \overline{Q_{26}} \\ 0 & 0 & \overline{Q_{44}} & \overline{Q_{45}} & 0 \\ 0 & 0 & \overline{Q_{54}} & \overline{Q_{55}} & 0 \\ \overline{Q_{61}} & \overline{Q_{62}} & 0 & 0 & \overline{Q_{66}} \end{bmatrix}_k \begin{Bmatrix} \varepsilon_x^f \\ \varepsilon_y^f \\ \gamma_{yz}^f \\ \gamma_{xz}^f \\ \gamma_{xy}^f \end{Bmatrix}_k \quad ,f = t,b \tag{12}$$

The core is considered as an orthotropic composite material, and the stress-strain relationships given by

$$\begin{Bmatrix} \sigma_x^c \\ \sigma_y^c \\ \tau_{yz}^c \\ \tau_{xz}^c \\ \tau_{xy}^c \end{Bmatrix} = \begin{bmatrix} \overline{Q_{11}} & \overline{Q_{12}} & 0 & 0 & 0 \\ \overline{Q_{21}} & \overline{Q_{22}} & 0 & 0 & 0 \\ 0 & 0 & \overline{Q_{44}} & 0 & 0 \\ 0 & 0 & 0 & \overline{Q_{55}} & 0 \\ 0 & 0 & 0 & 0 & \overline{Q_{66}} \end{bmatrix} \begin{Bmatrix} \varepsilon_x^c \\ \varepsilon_y^c \\ \gamma_{yz}^c \\ \gamma_{xz}^c \\ \gamma_{xy}^c \end{Bmatrix} \tag{13}$$

The efforts resultants of the core are obtained by integration of the stresses through the thickness direction of laminated plate

$$\begin{bmatrix} N_x & M_x & \overline{N_x} & \overline{M_x} \\ N_y & M_y & \overline{N_y} & \overline{M_y} \\ N_{xy} & M_{xy} & \overline{N_{xy}} & \overline{M_{xy}} \end{bmatrix} = \int_{-\frac{h_c}{2}}^{\frac{h_c}{2}} \begin{Bmatrix} \sigma_x \\ \sigma_y \\ \tau_{xy} \end{Bmatrix} \left(1, z, z^2, z^3\right) dz \tag{14}$$

$$\begin{bmatrix} V_x & S_x & R_x \\ V_y & S_y & R_y \end{bmatrix} = \int_{-\frac{h_c}{2}}^{\frac{h_c}{2}} \begin{Bmatrix} \tau_{xz} \\ \tau_{yz} \end{Bmatrix} \left(1, z, z^2\right) dz \tag{15}$$

where $N, M, \overline{N}$ and $\overline{M}$, denote membrane, bending moment, higher order membrane and higher order moment resultants respectively. V is the shear resultant; S and R are the higher order shear resultants.

By introducing the constitutive equation in the expressions of the resultant stress (14) and (15), the generalized constitutive equations become

$$\begin{Bmatrix} N \\ M \\ \overline{N} \\ \overline{M} \end{Bmatrix} = \begin{bmatrix} [A] & [B] & [D] & [E] \\ [B] & [D] & [E] & [F] \\ [D] & [E] & [F] & [G] \\ [E] & [F] & [G] & [H] \end{bmatrix} \begin{Bmatrix} \varepsilon^{(0)} \\ \chi^{(1)} \\ \chi^{(2)} \\ \chi^{(3)} \end{Bmatrix} \tag{16}$$

$$\begin{Bmatrix} V \\ S \\ R \end{Bmatrix} = \begin{bmatrix} [A^s] & [B^s] & [D^s] \\ [B^s] & [D^s] & [E^s] \\ [D^s] & [E^s] & [F^s] \end{bmatrix} \begin{Bmatrix} \gamma_s^{(0)} \\ \chi_s^{(1)} \\ \chi_s^{(2)} \end{Bmatrix} \tag{17}$$

where $N = \left(N_x \quad N_y \quad N_{xy}\right)^T, M = \left(M_x \quad M_y \quad M_{xy}\right)^T, \overline{N} = \left(\overline{N_x} \quad \overline{N_y} \quad \overline{N_{xy}}\right)^T, \overline{M} = \left(\overline{M_x} \quad \overline{M_y} \quad \overline{M_{xy}}\right)^T, V = \left(V_x \quad V_y\right)^T$, $S = \left(S_x \quad S_y\right)^T, R = \left(R_x \quad R_y\right)^T$.

The elements of the reduced stiffness matrices of the core $\left([A],\ [B], \text{etc.}\right)$ are defined by

$$\left(A_{ij}, B_{ij}, D_{ij}, E_{ij}, F_{ij}, G_{ij}, H_{ij}\right) = \int_{-\frac{h_c}{2}}^{\frac{h_c}{2}} \overline{Q}_{ij} \left(1, z, z^2, z^3, z^4, z^5, z^6\right) dz \qquad (i, j = 1, 2, 6) \tag{18}$$

and,

$$\left(A_{ij}^s, B_{ij}^s, D_{ij}^s, E_{ij}^s, F_{ij}^s\right) = \int_{-\frac{h_c}{2}}^{\frac{h_c}{2}} \overline{Q}_{ij} \left(1, z, z^2, z^3, z^4\right) dz \qquad (i, j = 4, 5) \tag{19}$$

According to the first order shear deformation theory, the elements of reduced stiffness matrices of the face-sheets are given by

Top face-sheet

$$\left(A_{ij}^t, B_{ij}^t, D_{ij}^t\right) = \int_{\frac{h_c}{2}}^{\frac{h_c}{2}+h_t} \overline{Q}_{ij}^{(k)} \left(1, z, z^2\right) dz = \sum_{k=1}^{nlayer} \int_{h^k}^{h^{k+1}} \overline{Q}_{ij}^{(k)} (1, z, z^2) dz \qquad (i, j = 1, 2, 6) \tag{20}$$

$$\left(\overline{A}_{ij}^{t}\right)=\int_{\frac{h_c}{2}}^{\frac{h_c}{2}+h_t}\overline{Q}_{ij}^{(k)}\,dz=\sum_{k=1}^{nlayer}\int_{h^k}^{h^{k+1}}\overline{Q}_{ij}^{(k)}dz \qquad (i,j=4,5) \tag{21}$$

Bottom face-sheet

$$\left(A_{ij}^{b},B_{ij}^{b},D_{ij}^{b}\right)=\int_{-\left(\frac{h_c}{2}+h_b\right)}^{-\frac{h_c}{2}}\overline{Q}_{ij}^{(k)}\left(1,z,z^2\right)dz=\sum_{k=1}^{nlayer}\int_{h^k}^{h^{k+1}}\overline{Q}_{ij}^{(k)}(1,z,z^2)dz \qquad (i,j=1,2,6) \tag{22}$$

$$\left(\overline{A}_{ij}^{b}\right)=\int_{-\left(\frac{h_c}{2}+h_b\right)}^{-\frac{h_c}{2}}\overline{Q}_{ij}^{(k)}\,dz=\sum_{k=1}^{nlayer}\int_{h^k}^{h^{k+1}}\overline{Q}_{ij}^{(k)}dz \qquad (i,j=4,5) \tag{23}$$

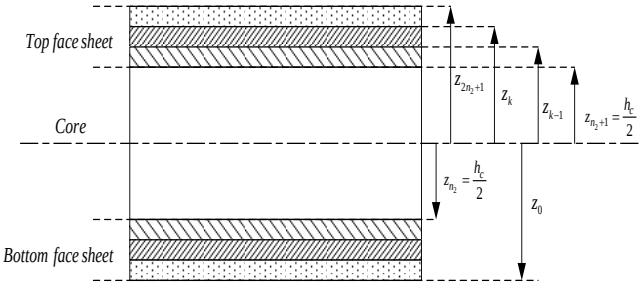

Fig.3
Coordinate locations of a sandwich plate having laminated composite faces.

3 FINITE ELEMENT FORMULATION

The present element, named RSFT52, is a C^0 continuous four-nodded Rectangular Sandwich plate element with thirteen DOF per node; based on the combination of the first order shear deformation theory and the third-order shear deformation plate theory. Each face-sheet has only two rotational DOF per node and the core has nine DOF per node: six rotational degrees and three translation components which are common for the all sandwich layers (Fig.4(a)).

The nodal displacement vector of the present element is defined by

$$\delta_i=\left\{u_i\;\; v_i\;\; w_i\;\; \psi_{xi}^{c}\;\; \psi_{yi}^{c}\;\; \eta_{xi}^{c}\;\; \eta_{yi}^{c}\;\; \zeta_{xi}^{c}\;\; \zeta_{yi}^{c}\;\; \psi_{xi}^{t}\;\; \psi_{yi}^{t}\;\; \psi_{xi}^{b}\;\; \psi_{yi}^{b}\right\}^T$$

The field variables may be expressed as follows

a. At mid-plate

$$u_0(x,y)=\sum_{i=1}^{4}N_i(x,y)\;u_{0i}\;\;;\;\;v_0(x,y)=\sum_{i=1}^{4}N_i(x,y)\;v_{0i}\;\;;\;\;w(x,y)=\sum_{i=1}^{4}N_i(x,y)\;w_{0i} \tag{24}$$

b. Core

$$\begin{aligned}&\psi_x^c(x,y)=\sum_{i=1}^{4}N_i(x,y)\psi_{xi}^{c},\qquad \psi_y^c(x,y)=\sum_{i=1}^{4}N_i(x,y)\psi_{yi}^{c},\qquad \eta_x^c(x,y)=\sum_{i=1}^{4}N_i(x,y)\eta_{xi}^{c}\\ &\eta_y^c(x,y)=\sum_{i=1}^{4}N_i(x,y)\eta_{yi}^{c},\qquad \zeta_x^c(x,y)=\sum_{i=1}^{4}N_i(x,y)\zeta_{xi}^{c},\qquad \zeta_y^c(x,y)=\sum_{i=1}^{4}N_i(x,y)\zeta_{yi}^{c}\end{aligned} \tag{25}$$

c. Top face-sheet

$$\psi_x^t(x,y)=\sum_{i=1}^{4}N_i(x,y)\psi_{xi}^t \quad , \qquad \psi_y^t(x,y)=\sum_{i=1}^{4}N_i(x,y)\psi_{yi}^t \tag{26}$$

d. Bottom face-sheet

$$\psi_x^b(x,y)=\sum_{i=1}^{4}N_i(x,y)\psi_{xi}^b \quad , \qquad \psi_y^b(x,y)=\sum_{i=1}^{4}N_i(x,y)\psi_{yi}^b \tag{27}$$

where N_i are the interpolation functions [48] associated with the node i (i = 1,2,3,4).

For the core, the generalized strain vector of the Eq. (2) at any point of coordinates (x, y) can be expressed in terms of nodal displacements as follows:

$$\begin{aligned}&\left\{\varepsilon^{(0)}\right\}^e=\left[B_\varepsilon^{(0)}\right]^{(e)}\left\{\delta_i\right\}_{(e)},\left\{\chi^{(1)}\right\}^e=\left[B_\chi^{(1)}\right]^{(e)}\left\{\delta_i\right\}_{(e)},\left\{\chi^{(2)}\right\}^e=\left[B_\chi^{(2)}\right]^{(e)}\left\{\delta_i\right\}_{(e)},\left\{\chi^{(3)}\right\}^e=\left[B_\chi^{(3)}\right]^{(e)}\left\{\delta_i\right\}_{(e)},\\&\left\{\gamma_s^{(0)}\right\}^e=\left[B_{\gamma_s}^{(0)}\right]^{(e)}\left\{\delta_i\right\}_{(e)},\left\{\chi_s^{(1)}\right\}^e=\left[B_{\chi_s}^{(1)}\right]^{(e)}\left\{\delta_i\right\}_{(e)},\left\{\chi_s^{(2)}\right\}^e=\left[B_{\chi_s}^{(2)}\right]^{(e)}\left\{\delta_i\right\}_{(e)}\end{aligned} \tag{28}$$

where the matrices $\left[B_\varepsilon^{(0)}\right],\left[B_\chi^{(1)}\right],\left[B_\chi^{(2)}\right],\left[B_\chi^{(3)}\right],\left[B_{\gamma_s}^{(0)}\right],\left[B_{\chi_s}^{(1)}\right]$ and $\left[B_{\chi_s}^{(2)}\right]$, are related the strains to nodal displacements.

For the top face-sheet, the generalized strain–displacement matrices given by

$$\left\{\varepsilon_m^t\right\}^e=\left[B_m^t\right]^e\left\{\delta_i\right\}_e,\left\{\varepsilon_f^t\right\}^e=\left[B_f^t\right]^e\left\{\delta_i\right\}_e,\left\{\gamma_s^t\right\}^e=\left[B_s^t\right]^e\left\{\delta_i\right\}_e \tag{29}$$

In the same way, the generalized strain–displacement matrices for the bottom face-sheet are

$$\left\{\varepsilon_m^b\right\}^e=\left[B_m^b\right]^e\left\{\delta_i\right\}_e,\left\{\varepsilon_f^b\right\}^e=\left[B_f^b\right]^e\left\{\delta_i\right\}_e,\left\{\gamma_s^b\right\}^e=\left[B_s^b\right]^e\left\{\delta_i\right\}_e \tag{30}$$

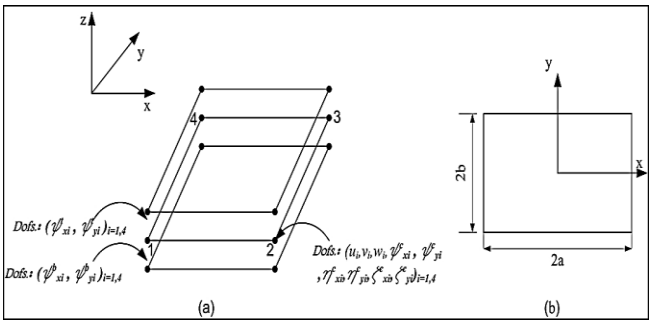

Fig.4
Geometry and corresponding degrees of freedom of the RSFT52 element.

3.1 Stiffness matrix

To establish the relationship between the forces and displacements, the principle of virtual work is used.

$$\delta\Pi=\delta U-\delta W=0 \tag{31}$$

Herein U indicates the total strain energy in the sandwich and W represents the work done by the external forces. δ denote the variation operator.

The total virtual strain energy of the three layers (top, core and bottom) may be written in the general form

$$\delta U = \delta U_c + \delta U_t + \delta U_b \tag{32}$$

where

$$\delta U = \int_v \left(\sigma^{(c)}\right)^T \delta\varepsilon^{(c)} dv + \int_v \left(\sigma^{(t)}\right)^T \delta\varepsilon^{(t)} dv + \int_v \left(\sigma^{(b)}\right)^T \delta\varepsilon^{(b)} dv \tag{33}$$

The thickness of the sandwich plate is assumed to remain unchanged and, accordingly, $\varepsilon_z = 0$. The expression for the strain energy (Eq. 33) simplifies to

$$\begin{aligned}
\delta U = & \int_{A_c} \int_{-\frac{h_c}{2}}^{\frac{h_c}{2}} \left(\sigma_{xx}^c \delta\varepsilon_{xx}^c + \sigma_{yy}^c \delta\varepsilon_{yy}^c + \sigma_{xy}^c \delta\varepsilon_{xy}^c + \sigma_{xz}^c \delta\varepsilon_{xz}^c + \sigma_{yz}^c \delta\varepsilon_{yz}^c\right) dz \; dA_c \\
& + \int_{A_t} \int_{\frac{h_c}{2}}^{\frac{h_c}{2}+h_t} \left(\sigma_{xx}^t \delta\varepsilon_{xx}^t + \sigma_{yy}^t \delta\varepsilon_{yy}^t + \sigma_{xy}^t \delta\varepsilon_{xy}^t + \sigma_{xz}^t \delta\varepsilon_{xz}^t + \sigma_{yz}^t \delta\varepsilon_{yz}^t\right) dz \; dA_t \\
& + \int_{A_b} \int_{-\left(\frac{h_c}{2}+h_b\right)}^{-\frac{h_c}{2}} \left(\sigma_{xx}^b \delta\varepsilon_{xx}^b + \sigma_{yy}^b \delta\varepsilon_{yy}^b + \sigma_{xy}^b \delta\varepsilon_{xy}^b + \sigma_{xz}^b \delta\varepsilon_{xz}^b + \sigma_{yz}^b \delta\varepsilon_{yz}^b\right) dz \; dA_b
\end{aligned} \tag{34}$$

The virtual work done by the external forces given by

$$\delta W = \int_{-b}^{+b} \int_{-a}^{+a} f\left(x, y\right) \delta w \; dxdy \tag{35}$$

In which $f\left(x, y\right)$ is the transverse static load.

a. Stiffness matrix of the core

By substituting the expressions of the stress resultants (Eqs. (16) and (17)) into the strain energy expression, the principle of virtual work for the core becomes

$$\begin{aligned}
\Pi_c = & \int_{-b}^{b} \int_{-a}^{a} \Big(\left\{\delta\varepsilon^{(0)}\right\}^T [A] \left\{\varepsilon^{(0)}\right\} + \left\{\delta\varepsilon^{(0)}\right\}^T [B] \left\{\chi^{(1)}\right\} + \left\{\delta\varepsilon^{(0)}\right\}^T [D] \left\{\chi^{(2)}\right\} + \left\{\delta\varepsilon^{(0)}\right\}^T [E] \left\{\chi^{(3)}\right\} \\
& + \left\{\delta\chi^{(1)}\right\}^T [B] \left\{\varepsilon^{(0)}\right\} + \left\{\delta\chi^{(1)}\right\}^T [D] \left\{\chi^{(1)}\right\} + \left\{\delta\chi^{(1)}\right\}^T [E] \left\{\chi^{(2)}\right\} + \left\{\delta\chi^{(1)}\right\}^T [F] \left\{\chi^{(3)}\right\} \\
& + \left\{\delta\chi^{(2)}\right\}^T [D] \left\{\varepsilon^{(0)}\right\} + \left\{\delta\chi^{(2)}\right\}^T [E] \left\{\chi^{(1)}\right\} + \left\{\delta\chi^{(2)}\right\}^T [F] \left\{\chi^{(2)}\right\} + \left\{\delta\chi^{(2)}\right\}^T [G] \left\{\chi^{(3)}\right\} \\
& + \left\{\delta\chi^{(3)}\right\}^T [E] \left\{\varepsilon^{(0)}\right\} + \left\{\delta\chi^{(3)}\right\}^T [F] \left\{\chi^{(1)}\right\} + \left\{\delta\chi^{(3)}\right\}^T [G] \left\{\chi^{(2)}\right\} + \left\{\delta\chi^{(3)}\right\}^T [H] \left\{\chi^{(3)}\right\} \\
& + \left\{\delta\gamma_s^{(0)}\right\}^T \left[A^s\right] \left\{\gamma_s^{(0)}\right\} + \left\{\delta\gamma_s^{(0)}\right\}^T \left[B^s\right] \left\{\chi_s^{(1)}\right\} + \left\{\delta\gamma_s^{(0)}\right\}^T \left[D^s\right] \left\{\chi_s^{(2)}\right\} + \left\{\delta\chi_s^{(1)}\right\}^T \left[B^s\right] \left\{\gamma_s^{(0)}\right\} \\
& + \left\{\delta\chi_s^{(1)}\right\}^T \left[D^s\right] \left\{\chi_s^{(1)}\right\} + \left\{\delta\chi_s^{(1)}\right\}^T \left[E^s\right] \left\{\chi_s^{(2)}\right\} + \left\{\delta\chi_s^{(2)}\right\}^T \left[D^s\right] \left\{\gamma_s^{(0)}\right\} + \left\{\delta\chi_s^{(2)}\right\}^T \left[E^s\right] \left\{\chi_s^{1}\right\} \\
& + \left\{\delta\chi_s^{(2)}\right\}^T \left[F^s\right] \left\{\chi_s^{(2)}\right\} \Big) dxdy - \int_{-b}^{b} \int_{-a}^{a} f \, \delta w \; dxdy = 0
\end{aligned} \tag{36}$$

with Eq. (28), the equilibrium equation can be expressed as follows

$$\left[K_e^{(c)}\right]\{d_e\} = \{f_e^{(c)}\} \tag{37}$$

where $\{f_e^{(c)}\}$ is the load vector for the core, $\left[K_e^{(c)}\right]$ is the element stiffness matrix of the core which may be defined by

$$\begin{aligned}
\left[K^{(c)}\right] = \sum_e \int_{-b}^{b}\int_{-a}^{a} (& \left[B_\varepsilon^{(0)}\right]^T [A]\left[B_\varepsilon^{(0)}\right] + \left[B_\varepsilon^{(0)}\right]^T [B]\left[B_\chi^{(1)}\right] + \left[B_\varepsilon^{(0)}\right]^T [D]\left[B_\chi^{(2)}\right] \\
& + \left[B_\varepsilon^{(0)}\right]^T [E]\left[B_\chi^{(3)}\right] + \left[B_\chi^{(1)}\right]^T [B]\left[B_\varepsilon^{(0)}\right] + \left[B_\chi^{(1)}\right]^T [D]\left[B_\chi^{(1)}\right] + \left[B_\chi^{(1)}\right]^T [E]\left[B_\chi^{(2)}\right] \\
& + \left[B_\chi^{(1)}\right]^T [F]\left[B_\chi^{(3)}\right] + \left[B_\chi^{(2)}\right]^T [D]\left[B_\varepsilon^{(0)}\right] + \left[B_\chi^{(2)}\right]^T [E]\left[B_\chi^{(1)}\right] + \left[B_\chi^{(2)}\right]^T [F]\left[B_\chi^{(2)}\right] \\
& + \left[B_\chi^{(2)}\right]^T [G]\left[B_\chi^{(3)}\right] + \left[B_\chi^{(3)}\right]^T [E]\left[B_\varepsilon^{(0)}\right] + \left[B_\chi^{(3)}\right]^T [F]\left[B_\chi^{(1)}\right] + \left[B_\chi^{(3)}\right]^T [G]\left[B_\chi^{(2)}\right] \\
& + \left[B_\chi^{(3)}\right]^T [H]\left[B_\chi^{(3)}\right] + \left[B_{\gamma_s}^{(0)}\right]^T \left[A^s\right]\left[B_{\gamma_s}^{(0)}\right] + \left[B_{\gamma_s}^{(0)}\right]^T \left[B^s\right]\left[B_{\chi_s}^{(1)}\right] + \left[B_{\gamma_s}^{(0)}\right]^T \left[D^s\right]\left[B_{\chi_s}^{(2)}\right] \\
& + \left[B_{\chi_s}^{(1)}\right]^T \left[B^s\right]\left[B_{\gamma_s}^{(0)}\right] + \left[B_{\chi_s}^{(1)}\right]^T \left[D^s\right]\left[B_{\chi_s}^{(1)}\right] + \left[B_{\chi_s}^{(1)}\right]^T \left[E^s\right]\left[B_{\chi_s}^{(2)}\right] \\
& + \left[B_{\chi_s}^{(2)}\right]^T \left[D^s\right]\left[B_{\gamma_s}^{(0)}\right] + \left[B_{\chi_s}^{(2)}\right]^T \left[E^s\right]\left[B_{\chi_s}^{(1)}\right] + \left[B_{\chi_s}^{(2)}\right]^T \left[F^s\right]\left[B_{\chi_s}^{(2)}\right]) dxdy
\end{aligned} \tag{38}$$

b. Stiffness matrix of the face sheets

The same steps are followed to elaborate the stiffness matrix of the two face sheets, therefore:

Top face-sheet

$$\begin{aligned}
\left[K^{(t)}\right] = \sum_e \int_{-b}^{b}\int_{-a}^{a} (& \underbrace{\left[B_m^t\right]^T \left[A^{(t)}\right]\left[B_m^t\right]}_{\text{membrane}} + \underbrace{\left[B_m^t\right]^T \left[B^{(t)}\right]\left[B_f^t\right]}_{\text{coupling membrane-bending}} + \underbrace{\left[B_f^t\right]^T \left[B^{(t)}\right]\left[B_m^t\right]}_{\text{coupling bending-membrane}} \\
& + \underbrace{\left[B_f^t\right]^T \left[D^{(t)}\right]\left[B_f^t\right]}_{\text{bending}} + \underbrace{\left[B_c^t\right]^T \left[A_c^{(t)}\right]\left[B_c^t\right]}_{\textit{shear}}) dxdy
\end{aligned} \tag{39}$$

Bottom-face sheet

$$\begin{aligned}
\left[K^{(b)}\right] = \sum_e \int_{-b}^{b}\int_{-a}^{a} (& \underbrace{\left[B_m^b\right]^T \left[A^{(b)}\right]\left[B_m^b\right]}_{\text{membrane}} + \underbrace{\left[B_m^b\right]^T \left[B^{(b)}\right]\left[B_f^b\right]}_{\text{coupling membrane-bending}} + \underbrace{\left[B_f^b\right]^T \left[B^{(b)}\right]\left[B_m^b\right]}_{\text{coupling bending-membrane}} \\
& + \underbrace{\left[B_f^b\right]^T \left[D^{(b)}\right]\left[B_f^b\right]}_{\text{bending}} + \underbrace{\left[B_c^b\right]^T \left[A_c^{(b)}\right]\left[B_c^b\right]}_{\textit{shear}}) dxdy
\end{aligned} \tag{40}$$

Finally, the total stiffness matrix $\left[K_T\right]$ of the element is given by

$$\left[K_T\right] = \left[K^{(t)}\right] + \left[K^{(c)}\right] + \left[K^{(b)}\right] \tag{41}$$

4 NUMERICAL RESULTS AND DISCUSSIONS

In this section, some problem of sandwich plates with laminated face sheets will be analyzed to assess the performance and applicability of the present finite element model. The obtained numerical results are compared with the analytical solutions given by Pagano [46], the experimental results obtained by Kanematsu et al. [47] and others finite elements numerical results found in literature. Table 1. shows the boundary conditions, for which the numerical results have been obtained, where CCCC, SSSS, CSCS and CFCF respectively indicate: clamped, simply supported, clamped-simply supported and clamped-free boundary conditions.

The following non-dimensional quantities used in the present analysis are defined as:

Non-dimensional transverse shear stresses

$$\left(\bar{\sigma}_{xz}, \bar{\sigma}_{yz}\right) = \frac{h}{q_0 a}\left(\sigma_{xz}, \sigma_{yz}\right) \tag{42}$$

Non-dimensional transverse displacement

$$\bar{w} = \left(\frac{100\ \mathrm{E}_2 h^3 w}{a^4 q_0}\right) \tag{43}$$

Table 1
Boundary conditions used in this study.

Boundary conditions	Abbreviations	Restrained edges
Simply supported	SSSS	$w_0 = \psi_x^c = \eta_x^c = \zeta_x^c = \psi_x^t = \psi_x^b = 0$ *at* $x = \pm\frac{a}{2}$ $w_0 = \psi_y^c = \eta_y^c = \zeta_y^c = \psi_y^t = \psi_y^b = 0$ *at* $y = \pm\frac{b}{2}$
Clamped	CCCC	$w_0 = \psi_x^c = \psi_y^c = \eta_x^c = \eta_y^c = 0$ $\zeta_x^c = \zeta_y^c = \psi_x^t = \psi_y^t = \psi_x^b = \psi_y^b = 0$
Clamped-Simply supported	CSCS	Clamped at $x = \pm\frac{a}{2}$ Simply supported at $y = \pm\frac{b}{2}$
Clamped-Free	CFCF	Clamped at $x = \pm\frac{a}{2}$ Free at $y = \pm\frac{b}{2}$

4.1 Square sandwich plate $(0/90/C/0/90)$ *having two-ply laminated stiff sheets at the faces with different boundary conditions*

In this example, an unsymmetrical square laminated sandwich plate, subjected to sinusoidal loading is studied. The thickness of each laminate layer is $0.05h$, whereas the thickness of the core is $0.8h$. The mechanical properties of materials used are listed in Table 2. Different thickness ratios (h/a = 0.01, 0.05, 0.1, 0.2, 0.25 and 0.5) and three types of boundary conditions (CCCC, SCSC and SSSS,) are taken into account. The values of non-dimensional transverse displacement and transverse shear stresses obtained in the present analysis are presented with those obtained from the literature [1, 18, 22, 49] in Table 3. The obtained results present a very good performance and also confirm the robustness of the RSFT52 element in terms of stability, rapidity of convergence and accuracy for both thin and thick plates.

Moreover, we also note when $h/a = 0.5$, the values of the transverse displacement are higher than those found with lower thickness ratios for both boundary conditions (CCCC and SCSC). This may be from the effect of

transverse flexibility of the core and shear deformation effects. Also, the thickness of the core ($0.8h$) which has an important role in the sandwich plates because, it considerably affects on the flexional rigidity.

Table 2
Material properties (normalized) used for laminated sandwiches plates.

Materials	Elastic properties					
	E_1	E_2	G_{12}	G_{13}	G_{23}	$\nu_{12}=\nu_{13}=\nu_{23}$
Core	0.04E	0.04E	0.016E	0.06E	0.06E	0.25
Face sheets	25E	E	0.5E	0.5E	0.2E	0.25

Table 3
Normalized maximum deflection ($\bar{w}$) and stresses ($\bar{\tau}_{xz}, \bar{\tau}_{yz}$) at the important points of square sandwich plate with laminated facings $(0/90/C/0/90)$ under distributed load of sinusoidal variation with different boundary conditions.

$\frac{h}{a}$	References	FE Models	$\bar{\tau}_{xz}\left(0,\frac{b}{2},0\right)$	$\bar{\tau}_{yz}\left(\frac{a}{2},0,0\right)$	$\bar{w}\left(\frac{a}{2},\frac{b}{2},0\right)$
Boundary condition: CCCC					
0.01	Present (8×8)	RSFT52	0.1877	0.1877	0.1075
	Present (12×12)	RSFT52	0.1981	0.1981	0.1519
	Present (16×16)	RSFT52	0.2008	0.2008	0.1778
	Khandelwal et al. [1]	FEM-Q9-HZZT[a]	0.2198	0.2190	0.2279
	Pandit et al. [18]	FEM-Q9-IHZZT	0.2189	0.2189	0.2286
	Singh et al. [49]	FEM-Q8-HZZT	0.2348	-	0.2260
	Chalak et al. [22]	FEM-Q9-HZZT	0.2171	0.2327	0.2267
0.05	Present (8×8)	RSFT52	0.1639	0.1639	0.4166
	Present (12×12)	RSFT52	0.1694	0.1694	0.4226
	Present (16×16)	RSFT52	0.1682	0.1682	0.4245
	Khandelwal et al. [1]	FEM-Q9-HZZT	0.1661	0.1661	0.4299
	Pandit et al. [18]	FEM-Q9-IHZZT	0.1828	0.1828	0.4296
	Singh et al. [49]	FEM-Q8-HZZT	0.2004	-	0.4462
	Chalak et al. [22]	FEM-Q9-HZZT	0.1568	0.2319	0.4283
0.1	Present (8×8)	RSFT52	0.1518	0.1518	1.0538
	Present (12×12)	RSFT52	0.1513	0.1513	1.0451
	Present (16×16)	RSFT52	0.1474	0.1474	1.0443
	Khandelwal et al. [1]	FEM-Q9-HZZT	0.1380	0.1383	1.0513
	Pandit et al. [18]	FEM-Q9-IHZZT	0.1587	0.1586	1.0489
	Singh et al. [49]	FEM-Q8-HZZT	0.1651	-	1.0213
	Chalak et al. [22]	FEM-Q9-HZZT	0.1308	0.2175	1.0484
0.2	Present (8×8)	RSFT52	0.1377	0.1377	3.4824
	Present (12×12)	RSFT52	0.1336	0.1336	3.4560
	Present (16×16)	RSFT52	0.1283	0.1283	3.4501
	Khandelwal et al. [1]	FEM-Q9-HZZT	0.1240	0.1242	3.4741
	Pandit et al. [18]	FEM-Q9-IHZZT	0.1396	0.1394	3.4521
	Singh et al. [49]	FEM-Q9-IHZZT	0.1422	-	3.3421
0.25	Present (8×8)	RSFT52	0.1325	0.1325	5.2499
	Present (12×12)	RSFT52	0.1279	0.1279	5.2157
	Present (16×16)	RSFT52	0.1227	0.1227	5.2046
	Khandelwal et al. [1]	FEM-Q9-HZZT	0.1228	0.1231	5.2470
	Chalak et al. [22]	FEM-Q9-HZZT	0.1157	0.1766	5.2305
0.5	Present (8×8)	RSFT52	0.1147	0.1147	18.9206
	Present (12×12)	RSFT52	0.1107	0.1107	18.7881
	Present (16×16)	RSFT52	0.1068	0.1068	18.7406
	Pandit et al. [18]	FEM-Q9-IHZZT[b]	0.1227	0.1217	18.3454
	Khandelwal et al. [1]	FEM-Q9-HZZT	0.1264	0.1265	19.1560
	Singh et al. [49]	FEM-Q8-HZZT[c]	0.1325	-	18.3450
	Chalak et al. [22]	FEM-Q9-HZZT	0.1182	0.1427	19.0444

[a] Nine-node quadratic finite element solution based on higher order zigzag plate theory.

Table 3
Continued.

$\frac{h}{a}$	References	FE Models	$\bar{\tau}_{xz}\left(0,\frac{b}{2},0\right)$	$\bar{\tau}_{yz}\left(\frac{a}{2},0,0\right)$	$\bar{w}\left(\frac{a}{2},\frac{b}{2},0\right)$
Boundary condition: SCSC					
0.01	Present (8×8)	RSFT52	0.0674	0.2774	0.1622
	Present (12×12)	RSFT52	0.0703	0.2859	0.2297
	Present (16×16)	RSFT52	0.0714	0.2868	0.2689
	Khandelwal et al. [1]	FEM-Q9-HZZT	0.0782	0.3061	0.3451
	Pandit et al. [18]	FEM-Q9-IHZZT	0.0778	0.3086	0.3453
	Singh et al. [49]	FEM-Q8-HZZT	0.0944	-	0.3920
	Chalak et al. [22]	FEM-Q9-HZZT	0.0775	0.3311	0.3430
0.05	Present (8×8)	RSFT52	0.0928	0.2301	0.5827
	Present (12×12)	RSFT52	0.0962	0.2357	0.5935
	Present (16×16)	RSFT52	0.0974	0.2333	0.5975
	Khandelwal et al. [1]	FEM-Q9-HZZT	0.1075	0.2288	0.6053
	Pandit et al. [18]	FEM-Q9-IHZZT	0.1061	0.2527	0.6052
	Singh et al. [49]	FEM-Q8-HZZT	0.1542	-	0.6080
	Chalak et al. [22]	FEM-Q9-HZZT	0.1012	0.3209	0.6022
0.1	Present (8×8)	RSFT52	0.1248	0.1893	1.2998
	Present (12×12)	RSFT52	0.1288	0.1881	1.2961
	Present (16×16)	RSFT52	0.1302	0.1830	1.2964
	Khandelwal et al. [1]	FEM-Q9-HZZT	0.1437	0.1711	1.3039
	Pandit et al. [18]	FEM-Q9-IHZZT	0.1418	0.1967	1.3026
	Singh et al. [49]	FEM-Q8-HZZT	0.1523	-	1.3096
	Chalak et al. [22]	FEM-Q9-HZZT	0.1366	0.2696	1.2994
0.2	Present (8×8)	RSFT52	0.1483	0.1524	3.8333
	Present (12×12)	RSFT52	0.1530	0.1476	3.8112
	Present (16×16)	RSFT52	0.1546	0.1418	3.8053
	Khandelwal et al. [1]	FEM-Q9-HZZT	0.1708	0.1369	3.8288
	Pandit et al. [18]	FEM-Q9-IHZZT	0.1683	0.1539	3.8087
	Singh et al. [49]	FEM-Q9-HZZT	0.1620	-	3.8500
0.25	Present (8×8)	RSFT52	0.1515	0.1436	5.6655
	Present (12×12)	RSFT52	0.1563	0.1384	5.6329
	Present (16×16)	RSFT52	0.1579	0.1326	5.6225
	Khandelwal et al. [1]	FEM-Q9-HZZT	0.1747	0.1327	5.6638
	Chalak et al. [22]	FEM-Q9-HZZT	0.1667	0.1907	5.6453
0.5	Present (8×8)	RSFT52	0.1490	0.1223	20.0912
	Present (12×12)	RSFT52	0.1538	0.1178	19.9625
	Present (16×16)	RSFT52	0.1555	0.1135	19.9181
	Pandit et al. [18]	FEM-Q9-IHZZT	0.1691	0.1296	19.5512
	Khandelwal et al. [1]	FEM-Q9-HZZT	0.1744	0.1338	20.3055
	Singh et al. [49]	FEM-Q8-HZZT	0.1721	-	19.5800
	Chalak et al. [22]	FEM-Q9-HZZT	0.1659	0.1512	20.1918

[b] Nine-node quadratic finite element solution based on improved higher order zigzag plate theory.
[c] Eight-nodes quadratic finite element solution based on higher order zigzag plate theory.

Table 3
Continued.

$\frac{h}{a}$	References	FE Models	$\bar{\tau}_{xz}\left(0,\frac{b}{2},0\right)$	$\bar{\tau}_{yz}\left(\frac{a}{2},0,0\right)$	$\bar{w}\left(\frac{a}{2},\frac{b}{2},0\right)$
Boundary condition: SSSS					
0.01	Present (8×8)	RSFT52	0.1787	0.1787	0.4285
	Present (12×12)	RSFT52	0.1797	0.1797	0.6010
	Present (16×16)	RSFT52	0.1791	0.1791	0.6996
	Pagano [46]	Elasticity solution	0.1773	0.1773	0.8888
	Khandelwal et al. [1]	FEM-Q9-HZZT	0.1878	0.1812	0.8782

0.1	Present (8×8)	RSFT52	0.1677	0.1677	1.7108
	Present (12×12)	RSFT52	0.1725	0.1725	1.7148
	Present (16×16)	RSFT52	0.1742	0.1742	1.7162
	Pagano [46]	Elasticity solution	0.1770	0.1770	1.7272
	Khandelwal et al. [1]	FEM-Q9-HZZT	0.1909	0.1883	1.7177
	Pandit et al. [18]	FEM-Q9-IHZZT	-	-	1.7252
	Chakrabarti and Sheikh [17]	FEM-T6-RHZZT	-	-	1.7249
	Chakrabarti and Sheikh [17]	FEM-T6-HZZT	-	-	1.6738
0.2	Present (8×8)	RSFT52	0.1666	0.1666	4.2552
	Present (12×12)	RSFT52	0.1715	0.1715	4.2380
	Present (16×16)	RSFT52	0.1732	0.1732	4.2320
	Pagano [46]	Elasticity solution	-	-	4.2447
	Pandit et al. [18]	FEM-Q9-IHZZT	-	-	4.2517
	Chakrabarti and Sheikh [17]	FEM-T6-RHZZT	-	-	4.2420
	Chakrabarti and Sheikh [17]	FEM-T6-HZZT	-	-	3.9798
0.25	Present (8×8)	RSFT52	0.1659	0.1659	6.1457
	Present (12×12)	RSFT52	0.1707	0.1707	6.1151
	Present (16×16)	RSFT52	0.1725	0.1725	6.1044
	Pagano [46]	Elasticity solution	0.1756	0.1756	6.1105
	Khandelwal et al. [1]	FEM-Q9-HZZT	0.1901	0.1888	6.1342

4.2 A square sandwich plate $(\theta/\theta+90/C/\theta/\theta+90)$ *with an angle-ply laminated stiff sheets at the two faces subjected to uniformly distributed load*

The same the geometrical and mechanical properties from the previous example has been adopted. The plate has a stratification of $(\theta/\theta+90/C/\theta/\theta+90)$ and subjected to a uniformly distributed load. In this example, three different types of meshes (8 × 8, 12 × 12 and 16 × 16) and three thickness ratios (h/a = 0.2, 0.1 and 0.05), are considered. The non-dimensional results of transverse displacement at the center of the plate $(x=a/2,\ y=b/2 \text{ et } z=0)$, the transverse shear stresses $(\bar{\tau}_{xz})$ at the center of the left edge $(x=0,\ y=a/2 \text{ et } z=\pm 0.4h)$ and the transverse shear stresses $(\bar{\tau}_{yz})$ at the center of the bottom edge $(x=a/2,\ y=0 \text{ et } z=\pm 0.4h)$ of the plate, obtained in the present analysis, for three orientation angles on the face sheets $(0^\circ,\ 30^\circ \text{ and } 45^\circ)$, are tabulated in Table 4. The results obtained by the present element RSFT52 are in excellent agreement with those obtained by Chakrabarti and Sheikh [17] et Khandelwal et al. [1].

Table 4

Normalized maximum deflection $(\bar{w})$ and transvers shear stresses $(\bar{\tau}_{xz}, \bar{\tau}_{yz})$ at the important points of a simply supported square sandwich plate with angle-ply laminated faces $(\theta/\theta+90/C/\theta/\theta+90)$ under uniformly distributed load.

$\frac{h}{a}$	References	FE Models	$\bar{\tau}_{xz}$	$\bar{\tau}_{yz}$	$\bar{w}$
$\theta=0^\circ$					
0.2	Present (8×8)	RSFT52	0.3033	0.3033	6.3228
	Present (12×12)	RSFT52	0.3242	0.3242	6.2940
	Present (16×16)	RSFT52	0.3343	0.3343	6.2909
	Pagano [46]	Elasticity solution	0.3436	0.3413	6.2981
	Khandelwal et al. [1]	FEM-Q9-HZZT (Const)*	0.3982	0.3993	6.3001
	Khandelwal et al. [1]	FEM-Q9-HZZT (Equil)**	0.3455	0.3332	6.3001
	Chakrabarti and Sheikh [17]	FEM-T6-HZZT	0.3482	-	6.3016
0.1	Present (8×8)	RSFT52	0.3110	0.3110	2.6104
	Present (12×12)	RSFT52	0.3337	0.3337	2.6149
	Present (16×16)	RSFT52	0.3447	0.3447	2.6168
	Pagano [46]	Elasticity	0.3496	0.3503	2.6168
	Khandelwal et al. [1]	FEM-Q9-HZZT (Const)	0.4142	0.4366	2.6295
	Khandelwal et al. [1]	FEM-Q9-HZZT (Equil)	0.3489	0.3397	2.6168
	Chakrabarti and Sheikh [17]	FEM-T6-HZZT	0.3612	-	2.6296

0.05	Present (8×8)	RSFT52	0.3176	0.3176	1.6419
	Present (12×12)	RSFT52	0.3408	0.3408	1.6766
	Present (16×16)	RSFT52	0.3522	0.3522	1.6891
	Pagano [46]	Elasticity	0.3560	0.3563	1.7107
	Khandelwal et al. [1]	FEM-Q9-HZZT (Const)	0.4515	0.5230	1.6957
	Khandelwal et al. [160]	FEM-Q9-HZZT (Equil)	0.3663	0.3612	1.6957
	Chakrabarti and Sheikh [17]	FEM-T6-HZZT	0.3732	-	1.7126
$\theta = 30^{\circ}$					
0.2	Present (8×8)	RSFT52	0.3185	0.3185	5.9480
	Present (12×12)	RSFT52	0.3382	0.3382	5.9326
	Present (16×16)	RSFT52	0.3472	0.3472	5.9308
	Khandelwal et al. [1]	FEM-Q9-HZZT (Const)	0.4376	0.4321	5.9579
	Khandelwal et al. [1]	FEM-Q9-HZZT (Equil)	0.3064	0.2951	5.9579
	Chakrabarti and Sheikh [17]	FEM-T6-HZZT	0.3762	-	5.9463
0.1	Present (8×8)	RSFT52	0.3211	0.3211	2.2081
	Present (12×12)	RSFT52	0.3406	0.3406	2.2137
	Present (16×16)	RSFT52	0.3503	0.3503	2.2176
	Khandelwal et al. [1]	FEM-Q9-HZZT (Const)	0.4280	0.4409	2.2322
	Khandelwal et al. [1]	FEM-Q9-HZZT (Equil)	0.3275	0.3200	2.2322
	Chakrabarti and Sheikh [17]	FEM-T6-HZZT	0.3659	-	2.2237
0.05	Present (8×8)	RSFT52	0.3261	0.3261	1.2028
	Present (12×12)	RSFT52	0.3465	0.3465	1.2199
	Present (16×16)	RSFT52	0.3570	0.3570	1.2270
	Khandelwal et al. [1]	FEM-Q9-HZZT (Const)	0.4637	0.5097	1.2450
	Khandelwal et al. [1]	FEM-Q9-HZZT (Equil)	0.3592	0.3480	1.2450
	Chakrabarti and Sheikh [17]	FEM-T6-HZZT	0.3603	0.3603	1.2381

* Values of transverse shear stresses obtained from constitutive relation.
** Values of transverse shear stresses obtained from equilibrium equations.

Table 4
Continued.

$\frac{h}{a}$	References	FE Models	$\bar{\tau}_{xz}$	$\bar{\tau}_{yz}$	$\bar{w}$
$\theta = 45^{\circ}$					
0.2	Present (8×8)	RSFT52	0.2955	0.2955	5.6998
	Present (12×12)	RSFT52	0.3144	0.3144	5.6615
	Present (16×16)	RSFT52	0.3231	0.3231	5.6516
	Khandelwal et al. [1]	FEM-Q9-HZZT (Const)	0.4612	0.4484	5.6329
	Khandelwal et al. [1]	FEM-Q9-HZZT (Equil)	0.3399	0.3187	5.6329
	Chakrabarti and Sheikh [17]	FEM-T6-HZZT	0.2197	-	5.6079
0.1	Present (8×8)	RSFT52	0.3025	0.3025	2.0132
	Present (12×12)	RSFT52	0.3223	0.3223	2.0035
	Present (16×16)	RSFT52	0.3320	0.3320	2.0019
	Khandelwal et al. [1]	FEM-Q9-HZZT (Const)	0.4445	0.4592	1.9950
	Khandelwal et al. [1]	FEM-Q9-HZZT (Equil)	0.3375	0.3232	1.9950
	Chakrabarti and Sheikh [17]	FEM-T6-HZZT	0.2203	-	1.9764
0.05	Present (8×8)	RSFT52	0.3034	0.3034	1.0615
	Present (12×12)	RSFT52	0.3215	0.3215	1.0671
	Present (16×16)	RSFT52	0.3311	0.3311	1.0697
	Khandelwal et al. [1]	FEM-Q9-HZZT (Const)	0.4621	0.5309	1.0773
	Khandelwal et al. [1]	FEM-Q9-HZZT (Equil)	0.3419	0.3335	1.0773
	Chakrabarti and Sheikh [17]	FEM-T6-HZZT	0.2197	-	1.0615

4.3 Comparison with experimental results CFRP-faced rectangular sandwich plates

The objective of this problem is to describe the practical application of the present element with the experimental results available in the literature. Kanematsu et al. [47] have performed out experiments on rectangular $(450\ mm \times 300\ mm)$ sandwich plates composed of CFRP face sheets and aluminum honeycomb core, for clamped

edge conditions. Each face sheet is symmetrically laminated with three carbon-epoxy layers, where the thickness of each layer is 0.125 *mm*. The mechanical properties of the plate are presented in Table 5. In this study, four different types (designated as SPl, SP2, SP3 and SP4) of stacking sequences, as shown in Fig. 5, for the faces of sandwich plate, are considered. The stacking sequences are: $[30/30/30]$, $[0/0/0]$, $[30/–30/30]$ and $[0/90/0]$, respectively, for SPl, SP2, SP3 et SP4. The thickness of the core is 10 *mm* for specimens SP1 and SP2, and 7 *mm* for specimens SP3 and SP4. The plate is subjected to a uniformly distributed load P = 1,010 *KPa*. This load is controlled by a manometer and the transverse displacement of the plate was measured with a linearly variable differential transducer (LVDT). A holographic technique is used in order to visualize the transverse displacement modes.

Furthermore, the authors also have provided analytical solutions, based on the Rayleigh-Ritz method, for the same problem of plate, using two types of boundary conditions, simply supported (SSSS) and clamped (CCCC). The results of transverse displacement (w), obtained from the present element, are presented in Table 6., using a mesh size of (16 × 16). The comparison was made with the analytical solutions given by Kanematsu et al. [47], the solutions based on experimental works presented by the same authors [47], as well as with the finite element models of Lee et Fan [28] and Nayak et al.[13]. The results of the comparison show the effectiveness and reliability of the present element in the analysis of this type of structures.

Table 5
Material properties for Sandwich plates.

Materials	Elastic properties (GPa)					
	E_1	E_2	G_{12}	G_{13}	G_{23}	$\nu_{12}=\nu_{13}=\nu_{23}$
Carbon/epoxy	105	8.74	4.56	4.56	4.56	0.327
Al/Honeycomb	0.0686	0.0686	0.0264	0.103	0.621	0.3

Table 6
Deflexion (w) of three-layer rectangular sandwich plates under uniform load.

Reference	FE Models	Central displacement $w\left(\frac{a}{2},\frac{b}{2},0\right)(mm)$			
		SP1	SP2	SP3	SP4
Boundary condition: CCCC					
Present element	RSFT52	0.04906	0.05647	0.07506	0.05525
Nayak et al.[14]	FEM-Q9-HSDT[d]	-	0.05248	-	0.05797
Kanematsu et al. [47]	Analytical solution	0.05040	0.05400	0.07720	0.06130
Kanematsu et al. [47]	Experimental solution	0.06900	0.08500	0.09400	0.09000
Lee et Fan [28]	FEM-Q9-LWT	0.05190	0.05524	0.07834	0.06216
Boundary condition: SSSS					
Present element	RSFT52	0.1160	0.1733	0.1695	0.2010
Nayak et al.[14]	FEM-Q9-HSDT	-	0.1754	-	0.2111
Kanematsu et al. [47]	Analytical solution	0.1173	0.1829	0.1794	0.2206
Lee et Fan [28]	FEM-Q9-LWT[e]	0.1213	0.1774	0.1729	0.2138

[d] Nine-node quadratic finite element solution based on higher order shear deformation plate theory
[e] Nine-node quadratic finite element solution based on layer wise plate theory

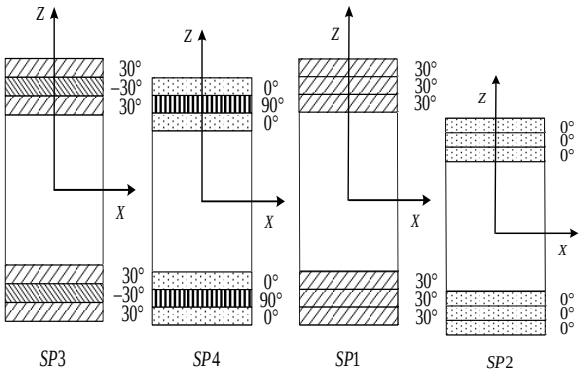

Fig.5
Sandwich plate cross sections.

4.4 Influence of the material and geometric properties on the transverse displacement

After verifying the accuracy and efficiency of the element against the known cases in the literature, we present below a parametric study to further understand the bending behaviour of sandwich plates having laminated composites face sheets.

This study aims to demonstrate the influence and evolution of different parameters (core thickness, side-to-thickness ratio, boundary conditions, aspect ratio, core-face sheet anisotropy ratio and degree of orthotropy of the face sheet) on the transverse displacement. The analysis is carried out for a square sandwich plate $(0/90/0/C/0/90/0)$ subjected to sinusoidal loading and a thickness ratio $(a/h=10)$, where h is the total thickness of the plate. The core is made of HEREX-C70.130 closed-cell PVC (polyvinyl chloride) foam and the face sheets are made of glass fiber in polyester resin. The mechanical properties of the face sheets and the core can be found in Table 7. [50]. The thickness of the core is 7 *mm*, while the face sheets are considered as symmetric cross-ply laminates $[0/90/0]$, where the thickness of each layer is 0.125 *mm.*

Table 7
The material properties of glass fiber and ester resin matrix.

Materials	Elastic properties (GPa)						
	E_1	E_2	G_{12}	G_{13}	G_{23}	$\nu_{12}=\nu_{13}$	ρ (Kg/m^3)
Glass / polyester	24.51	7.77	3.34	3.34	1.34	0.078	1800
HEREX-C70.130 foam	0.1036	0.1036	0.05	0.05	0.32	0.3	130

The curves of Fig.6 show the effect of the relative thickness of the core (h_c), represented by the ratio (h_c/h), on the non-dimensional transverse displacement $(\overline{w})$, with different type of boundary conditions (SSSS, CCCC, CFCF and CSCS). It can be seen that the values of transverse displacement increases with increasing (h_c/h) ratio, whatever boundary conditions. This elevation is probably due to the decrease of the flexural rigidity.

The variation of the non-dimensional transverse displacement $(\overline{w})$ with different thickness ratios (a/h), has been plotted as shown in Fig.7, for the two cases of boundary conditions; simply supported (SSSS) and clamped (CCCC). It was seen that, for both boundary conditions, the values of transverse displacement decreases with increased a/h ratio up to $a/h=20$ and then varies constantly in all cases. This can be explained by the effects of shear deformation and transverse flexibility of the core, which are more significant when the thickness increases. Furthermore, the core occupies major portion (90%) of the plate thickness, so the core compressibility plays very important role for highly thick plates.

The influence of aspect ratio (a/b) on the non-dimensional transverse displacement of a simply supported sandwich plate, is presented in Fig. 8. It is found that the variation of the transverse displacement decrease with increase in aspect ratio.

The next part concerns the study of the effect of the core-to-face sheet anisotropy ratio (E_1/E_c), of one part, and the ratio of the core shear modulus to the flexural modulus (G_c/E_c), of the other part, on the non-dimensional transverse displacement of a simply supported sandwich plate. In this study, the Young's modulus of the core (E_c) has been varied for each test, while the Young's modulus of the face sheet (E_1) is fixed. As shown in Fig. 9, the curves demonstrated that the transverse displacement is affected considerably by the variation of the modular ratio (E_1/E_c). It observed that, the values of the transverse displacement increase when the values of the anisotropy ratio increases, whatever the (G_c/E_c) ratio. This increase is probably due to the decrease in flexural stiffness caused by excess material of the core.

Fig.10 shows the effect of the degree of orthotropy of the faces (E_1/E_2) and the ratio h_c/h , on the non-dimensional transverse displacement $(\overline{w})$, of a simply supported sandwich plate. From Fig. 10, it can be seen that, for different core thickness (h_c/h), the non-dimensional central deflection decrease with increase of the degree of orthotropy of the faces. It is a well-known fact, from the literature, that an increase in the stiffness of a sandwich plate leads to a decrease in its transverse displacement. A stiffness increase could be due to a decrease in the relative thickness of the core or to an increase in the degree of orthotropy of the faces.

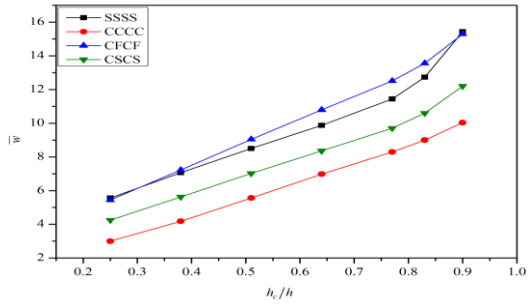

Fig.6
Effect of core thickness on the non-dimensional transverse displacement, of a sandwich plate $(0/90/0/C/0/90/0)$ with different boundary conditions.

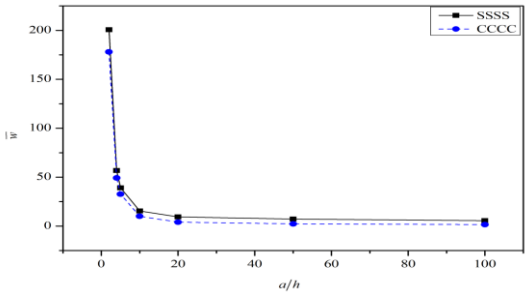

Fig.7
Effect of plate side-to-thickness ratio, a/h, on the non-dimensional transverse displacement, of a sandwich plate $(0/90/0/C/0/90/0)$ with two types of boundary conditions (SSSS and CCCC).

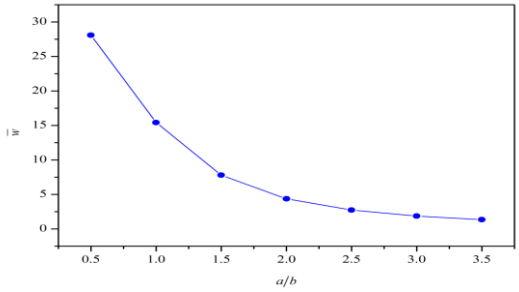

Fig.8
Effect of plate aspect ratio, a/b, on the non-dimensional transverse displacement, of a simply supported sandwich plate $(0/90/0/C/0/90/0)$.

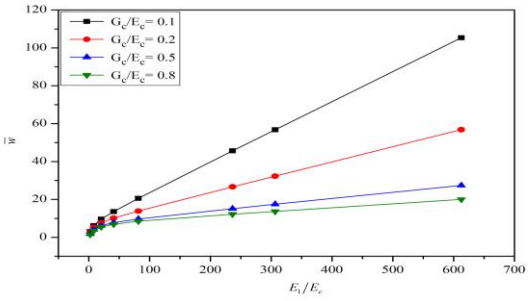

Fig.9
Effect of the modulus ratio, E_1/E_c, and ratio G_c/E_c, on the non-dimensional transverse displacement, of a simply supported sandwich plate $(0/90/0/C/0/90/0)$.

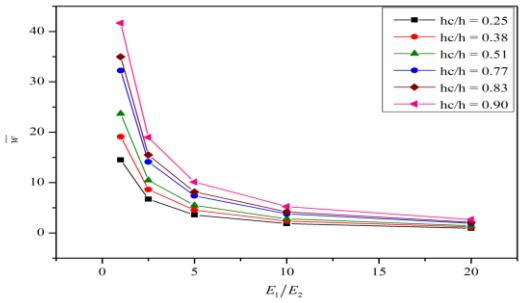

Fig.10
Effect of the degree of orthotropy of the face sheet, E_1/E_2, and ratio h_c/h, on the non-dimensional transverse displacement, of a simply supported sandwich plate $(0/90/0/C/0/90/0)$.

5 CONCLUSIONS

In this paper, a study of bending behaviour of composites sandwich plates with laminated face sheets has been undertaken, using a new four-nodded rectangular finite element formulation based on a layer-wise theory. The model is based on a proper combination of higher order and first order, shear deformation theories. Compatibility conditions as well as continuity of displacements, at the interface have been explicitly satisfied in the present formulation. Although the model is a layer-wise one, the number of unknowns is independent of the number of layers. Thus, the plate theory enjoys the advantage of a single-layer plate theory, even though it is based on the concept of a layer-wise plate approach. The results obtained for the transverse displacement and the transvers shear stresses, of a composite sandwich plate show very good performance of the present formulation. Hence, the potential of the element can be used to generate a number of new results, which are expected to be useful to the future research in this field.

In addition, the parametric effects of core thickness, side-to-thickness ratio, boundary conditions, plate aspect ratio, core-to-face sheet anisotropy ratio, core shear modulus to the flexural modulus ratio and degree of orthotropy of the face sheet, on the transverse displacement are discussed. The results reaffirm that these effects play an important role in the transverse displacement of composite sandwich plates with laminated face sheets.

REFERENCES

[1] Khandelwal R., Chakrabarti A., Bhargava P., 2013, An efficient FE model based on combined theory for the analysis of soft core sandwich plate, *Computational Mechanics* **51**(5): 673-697.

[2] Kant T., Swaminathan K., 2000, Estimation of transverse/interlaminar stresses in laminated composites – a selective review and survey of current developments, *Composite Structures* **49**(1): 65-75.

[3] Kirchhoff G., 1850, Über das gleichgewicht und die bewegung einer elastischen scheibe, *Journal für die Reine und Angewandte Mathematik* **40**: 51-88.

[4] Librescu L., 1975, *Elastostatics and Kinetics of Anisotropic and Heterogeneous Shell-Type Structures*, Noordhoff, Leyden, Netherlands.

[5] Ounis H., Tati A., Benchabane A., 2014, Thermal buckling behavior of laminated composite plates: a finite-element study, *Frontiers of Mechanical Engineering* **9**(1): 41-49.

[6] Stavsky Y., 1965, On the theory of symmetrically heterogeneous plates having the same thickness variation of the elastic moduli, *Topics in Applied Mechanics* 105-166.

[7] Reissner E., 1975, On transverse bending of plates, including the effect of transverse shear deformation, *International Journal of Solids and Structures* **11**(5): 569-573.

[8] Whitney J., Pagano N., 1970, Shear deformation in heterogeneous anisotropic plates, *Journal of Applied Mechanics* **37** (4) : 1031-1036.

[9] Mindlin R., 1951, Influence of rotary inertia and shear on flexural motions of isotropic, elastic plates, *Journal of Applied Mechanics* **18** :31-38.

[10] Yang P.C., Norris C.H., Stavsky Y., 1966, Elastic wave propagation in heterogeneous plates, *International Journal of Solids and Structures* **2**(4): 665-684.

[11] Lo K., Christensen R., Wu E., 1977, A high-order theory of plate deformation-part 2: laminated plates, *Journal of Applied Mechanics* **44**(4) : 669-676.

[12] Manjunatha B., Kant T., 1993, On evaluation of transverse stresses in layered symmetric composite and sandwich laminates under flexure, *Engineering Computations* **10**(6): 499-518.

[13] Nayak A., Moy S.J., Shenoi R., 2003, Quadrilateral finite elements for multilayer sandwich plates, *The Journal of Strain Analysis for Engineering Design* **38**(5): 377-392.

[14] Reddy J.N., 1984, A simple higher-order theory for laminated composite plates, *Journal of Applied Mechanics* **51**(4): 745-752.

[15] Rezaiee-Pajand M., Shahabian F., Tavakoli F., 2012, A new higher-order triangular plate bending element for the analysis of laminated composite and sandwich plates, *Structural Engineering and Mechanics* **43**(2): 253-271.

[16] Tu T.M., Thach L.N., Quoc T.H., 2010, Finite element modeling for bending and vibration analysis of laminated and sandwich composite plates based on higher-order theory, *Computational Materials Science* **49**(4) S390-S394.

[17] Chakrabarti A., Sheikh A.H., 2005, Analysis of laminated sandwich plates based on interlaminar shear stress continuous plate theory, *Journal of Engineering Mechanics* **131**(4): 377-384.

[18] Pandit M.K., Sheikh A.H., Singh B.N., 2008, An improved higher order zigzag theory for the static analysis of laminated sandwich plate with soft core, *Finite Elements in Analysis and Design* **44**(9): 602-610.

[19] Carrera E., 2003, Historical review of zig-zag theories for multilayered plates and shells, *Applied Mechanics Reviews* **56**: 287-308.

[20] Cho M., Parmerter R., 1993, Efficient higher order composite plate theory for general lamination configurations, *AIAA Journal* **31**(7): 1299-1306.
[21] Di Sciuva M., 1986, Bending vibration and buckling of simply supported thick multilayered orthotropic plates: an evaluation of a new displacement model, *Journal of Sound and Vibration* **105**(3): 425-442.
[22] Chalak H.D., 2012 , An improved C0 FE model for the analysis of laminated sandwich plate with soft core, *Finite Elements in Analysis and Design* **56**: 20-31.
[23] Kapuria S., Nath J., 2013, On the accuracy of recent global–local theories for bending and vibration of laminated plates, *Composite Structures* **95**: 163-172.
[24] Li X., Liu D., 1997, Generalized laminate theories based on double superposition hypothesis, *International Journal for Numerical Methods in Engineering* **40**(7) : 1197-1212.
[25] Wu Z., Chen R., Chen W., 2005, Refined laminated composite plate element based on global–local higher-order shear deformation theory, *Composite Structures* **70**(2) : 135-152.
[26] Zhen W., Wanji C., 2010, A C0-type higher-order theory for bending analysis of laminated composite and sandwich plates, *Composite Structures* **92**(3): 653-661.
[27] Shariyat M., 2010, A generalized global–local high-order theory for bending and vibration analyses of sandwich plates subjected to thermo-mechanical loads, *International Journal of Mechanical Sciences* **52**(3): 495-514.
[28] Lee L. Fan Y., 1996, Bending and vibration analysis of composite sandwich plates, *Computers and Structures* **60**(1): 103-112.
[29] Linke M., Wohlers W., Reimerdes H.G., 2007, Finite element for the static and stability analysis of sandwich plates, *Journal of Sandwich Structures and Materials* **9**(2): 123-142.
[30] Mantari J., Oktem A., Guedes Soares C., 2012, A new trigonometric layerwise shear deformation theory for the finite element analysis of laminated composite and sandwich plates, *Computers and Structures* **94**: 45-53.
[31] Oskooei S., Hansen J., 2000, Higher-order finite element for sandwich plates, *AIAA Journal* **38**(3): 525-533.
[32] Plagianakos T.S., Saravanos D.A., 2009, Higher-order layerwise laminate theory for the prediction of interlaminar shear stresses in thick composite and sandwich composite plates, *Composite Structures* **87**(1): 23-35.
[33] Ramesh S.S., 2009, A higher-order plate element for accurate prediction of interlaminar stresses in laminated composite plates, *Composite Structures* **91**(3): 337-357.
[34] Reddy J.N., 1987, A generalization of two-dimensional theories of laminated composite plates, *Communications in Applied Numerical Methods* **3**(3): 173-180.
[35] Wu C. P., Lin C. C., 1993, Analysis of sandwich plates using a mixed finite element, *Composite Structures* **25**(1): 397-405.
[36] Maturi D.A., 2014, Analysis of sandwich plates with a new layerwise formulation, *Composites Part B: Engineering* **56**: 484-489.
[37] Phung-Van P., 2014, Static and free vibration analyses of composite and sandwich plates by an edge-based smoothed discrete shear gap method (ES-DSG3) using triangular elements based on layerwise theory, *Composites Part B: Engineering* **60**: 227-238.
[38] Reddy J.N., 1993, An evaluation of equivalent-single-layer and layerwise theories of composite laminates, *Composite Structures* **25**(1-4): 21-35.
[39] Carrera E., 2002, Theories and finite elements for multilayered, anisotropic, composite plates and shells, *Archives of Computational Methods in Engineering* **9**(2): 87-140.
[40] Ha K., 1990, Finite element analysis of sandwich plates: an overview, *Computers and Structures* **37**(4): 397-403.
[41] Khandan R., 2012, The development of laminated composite plate theories: a review, *Journal of Materials Science* **47** (16): 5901-5910.
[42] Noor A.K., Burton W.S., Bert C.W., 1996, Computational models for sandwich panels and shells, *Applied Mechanics Reviews* **49**: 155-199.
[43] Zhang Y., Yang C., 2009, Recent developments in finite element analysis for laminated composite plates, *Composite Structures* **88**(1): 147-157.
[44] Ramtekkar G., Desai Y., Shah A., 2002, Mixed finite-element model for thick composite laminated plates, *Mechanics of Advanced Materials and Structures* **9**(2): 133-156.
[45] Ramtekkar G., Desai Y., Shah A., 2003, Application of a three-dimensional mixed finite element model to the flexure of sandwich plate, *Computers and Structures* **81**(22): 2183-2198.
[46] Pagano N., 1970, Exact solutions for rectangular bidirectional composites and sandwich plates, *Journal of Composite Materials* **4**(1): 20-34.
[47] Kanematsu H.H., Hirano Y., Iyama H., 1988, Bending and vibration of CFRP-faced rectangular sandwich plates, *Composite Structures* **10**(2): 145-163.
[48] Zienkiewicz O.C., Taylor R.L., 2000, *The Finite Element Method: Solid Mechanics*, Butterworth-heinemann.
[49] Singh S.K., 2011, An efficient C0 FE model for the analysis of composites and sandwich laminates with general layup, *Latin American Journal of Solids and Structures* **8**(2): 197-212.
[50] Meunier M., Shenoi R., 1999, Free vibration analysis of composite sandwich plates, *Proceedings of the Institution of Mechanical Engineers, Part C: Journal of Mechanical Engineering Science* **213**(7): 715-727.